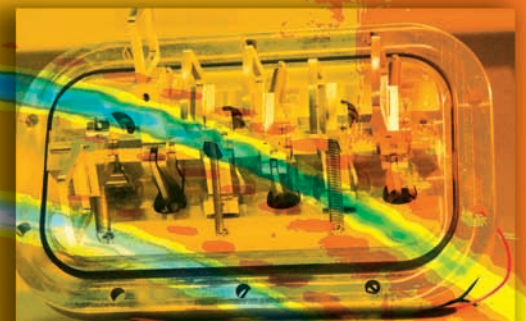
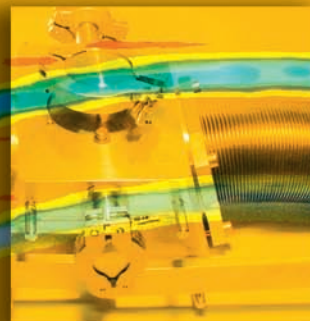


XMaS

NEWSLETTER



2007



contents



3 **User meeting**

4 **Instrumental developments**

6 **Some recent experiments**

14 **News round-up**

15 **Guidelines for applying for beam-time at the XMaS beamline**

XMaS had the best possible news in May 2007 when we heard that our application for the 5 year period, September 2007-12, was to be funded. This was by no means a foregone conclusion; in fact as far as we can work out our application was the only one funded in that EPSRC round of largescale applications. It is a tremendous accolade to everyone that our peers think XMaS science is so good: everyone associated with the beamline and its ongoing programme should have opened at least one bottle of champagne to celebrate (but please do not send us the bill!).

Now we have to get on with the work and that of course means not just continuing to do the same as before but launching the new ventures we proposed. The biggest instrumental project is to provide cryo-cooling for the monochromator. Those of you who were at our Users' Meeting in Liverpool last November will know that we have continued to think long and hard about this. It is difficult to predict whether the increase in beam current will simply increase our photon flux pro-rata or actually cause further deterioration in the flux and spot size due to the additional heating. We do know that at present we are losing about half the potential flux and have a focal spot that is somewhat larger than it might be, but a factor of two by itself never made the crucial difference in any experiment. One thing is certain, and that is we must ensure we can quickly get back to the current water-cooled system if we experience difficulties with cryo-cooling. We are going ahead but it will be a slow and expensive venture. For one thing the cooling system has a long delivery time and it can only be installed during a major shut down, the next complication is that the optics hutch itself needs to be altered if we are going to be able to get the "not very bendy" liquid nitrogen pipes into the monochromator vessel and still be able to open it to get to the crystal cage. We had not thought of that

complication beforehand and we are now working on affordable as well as workable solutions.

The second project is to extend the operation to lower energies by improving the vacuum and removing windows etc. when we want to access the lower energies: this is described later in this Newsletter and takes advantage of the XMaS team's latest bright idea for filters and attenuator!

Just a few words of caution before we get too euphoric: you might have noticed that the Euro is rising steadily in value against sterling, it has appreciated by over 10% since we submitted the grant application and it is likely that the slide of the pound against the Euro will continue for some time.

A lot of XMaS costs are inevitably in Euros and so this trend is bad news. Our budget is in pounds sterling and we have no contingency for currency fluctuations, except to be prudent and not to waste money! At the time of writing we are also still unclear about the schedule for the implementation of ESRF's Upgrade Programme, which will certainly disrupt our operation. The PLUO will disappear and, although the beamline itself should not be directly affected, access to it may be impossible when other building work is in progress. Obviously we are keeping a watchful eye on these developments.

Now for some more cheerful notes. We were delighted that Danny Mannix obtained one of the much soughtafter CNRS posts. Since November he has been installed in the Institut Néel, just down the road and so he has not entirely disappeared off the XMaS scene. His replacement is not exactly a newcomer, Peter Normile is another product of the Liverpool University Condensed Matter Physics Group, having been Bill Stirling's PhD student over a decade ago. He comes back to XMaS from a postdoc position in University of CastillaLa Mancha, where he was working on nanomagnetic materials. Sometime soon we should be appointing to a joint position funded by XMaS (2 yrs at XMaS) and the DIAMOND Light Source (a further 2 yrs at DIAMOND). This will further research collaborations between ourselves and associated beamlines on the UK machine.

Finally we are very pleased to announce that our 2008 users' Meeting will be incorporated into the overall UK SR Users' Meeting on Thursday 11th and Friday 12th September, which will be held at Daresbury. ■

Malcolm Cooper and Chris Lucas.



XMaS user meeting in November



The annual XMaS Users' Meeting was held in the Department of Physics at the University of Liverpool on Wednesday 28th November 2007. The meeting attracted approximately 40 participants representing 12 UK institutions and was also attended by our EPSRC contact, Simon Crook. Following an introductory welcome by Chris and Malcolm, the morning session consisted of some lively user presentations giving a flavour of the breadth of science that is performed on the beamline.

Professor Brian Tanner (Durham) started the session by describing some recent results relating magnetotransport properties to structure in room temperature spintronic materials and illustrating the complementarity between XMaS and I16 at the Diamond Light Source. Dr Danny Mannix then showed some highlights of his work on multiferroic materials. Dr Xiangbing Zeng (Sheffield) gave a fascinating talk in which he described use of the MAR CCD detector to perform grazing incidence small angle scattering (GISAXS) studies of liquid crystals and liquid crystal nanocomposites. The morning session was concluded with a talk by Professor Mark Dowsett (Warwick) describing recent results and future plans for cultural heritage studies using XMaS and other beamlines at the ESRF.

The afternoon session began with three talks describing the more conventional use of the beamline to perform resonant x-ray diffraction studies. Professor Jon Goff (Royal Holloway), back on familiar territory in Liverpool, presented a study of the orbital ordering in GdVO₃ which provoked an interesting audience debate regarding the interpretation of the results. Dr Emilio Lorenzo (CNRS) presented a resonant diffraction study of ordering in strongly correlated compounds and Dr Ross Springell (ESRF) described the use of resonant techniques to probe the induced magnetism in uranium metal. Paul Thompson (XMaS team) then described the recent beamline developments and presented the possible options with regard to the upgrading of the monochromator. This was discussed in detail by the audience. Steve Collins (Diamond) finished off the afternoon session by highlighting recent developments on I16 at Diamond.

Following a tea break the meeting was concluded by a stimulating presentation by Professor Roger Cowley (Oxford) – featured in the picture – below,

who was honoured by the IOP in 2008 by the award of the Faraday medal for pioneering work in the development and application of neutron and X-ray scattering techniques to the physics of a wide range of important solid and liquidstate systems. In his presentation, Roger described new possibilities in inelastic scattering, nanotechnology and coherence, indicating how new techniques can give insight into some longstanding problems and also discussing some of the issues relevant to the long term strategy currently under development at the ESRF.

The participants departed having spent a day hearing both about the science performed on the XMaS beamline and the latest opportunities in x-ray diffraction and scattering that are available to UK scientists at synchrotron radiation facilities. In order to stress the importance of the XMaS beamline in the portfolio of synchrotron facilities available to UK users, next year's XMaS annual User' Meeting will be incorporated into the UK Synchrotron Radiation User Meeting that is scheduled to take place on September 11-12, 2008 at the Daresbury Laboratories. Please put the date into your diaries!



Monochromator upgrade

The monochromator installed on the XMaS beamline was originally designed to operate between 3 – 15 KeV. Three years ago, this was modified to allow operation at lower energies and experiments have since been performed at the sulphur K edge (2.47 KeV). We propose installing a new cryogenically cooled monochromator which should enable operation down to 2.2 KeV. Under consideration are two designs from different manufacturers, one from a company that has recently supplied cryogenically cooled monochromators to the ESRF and the other from the company that supplied our present water-cooled monochromator. The detailed assessment of these designs continues.

Improved low-energy performance

Apart from the mechanical difficulties of designing a monochromator to cope with these high angles for low energy operation, another major problem is absorption due to air and vacuum windows. There is currently 350 m of beryllium downstream of the beamline front end window (500 m). One window separates the monochromator and the mirror vacuum and the other separates the high vacuum sections of the beamline from the lower vacuum area in the experimental hut. The removal of these two windows for low energy experiments would give an increase in flux of nearly two orders of magnitude at energies below 3 KeV. We are actively exploring the possibilities of mounting these windows into gate valves, so that the beamline enjoys the protection of the windows for the majority higher energy

experiments and then be removed for the softer energy experiments.

It will be essential, then, to improve the vacuum environment for the incident flight tube in the experiment hut, as this was originally designed to be low/medium vacuum only. Some improvements, such as replacing all kapton windows with beryllium are easily implemented. However, it will be necessary to change the commercial pneumatically operated attenuator units, since they are inherently incapable of high vacuum operation and are, anyway, becoming unreliable, through wear. A new attenuator system has been designed and built that incorporates no vacuum mechanical or electrical feedthroughs. The attenuator movement is based upon a solenoid/lever system with the positions read from magnetic reed switches. As now, the system is driven under SPEC or manual control.

This philosophy for the flight path must also apply for the detectors. The elimination/reduction of windows and air paths has the potential to provide a further order of magnitude saving in flux in the sub-3keV energy regime. Having a detector with good energy resolution, that allows samples to be aligned with high energy harmonics, is also a useful facility. A silicon drift diode detector seems the ideal candidate and investigations are currently being made to reduce the window thickness on these detectors. Recently, the beamline team have also collaborated with Cyberstar SA in the re-engineering of the avalanche photodiode (APD) package, resulting in a version mounted onto a vacuum flange, thereby minimising air gaps.

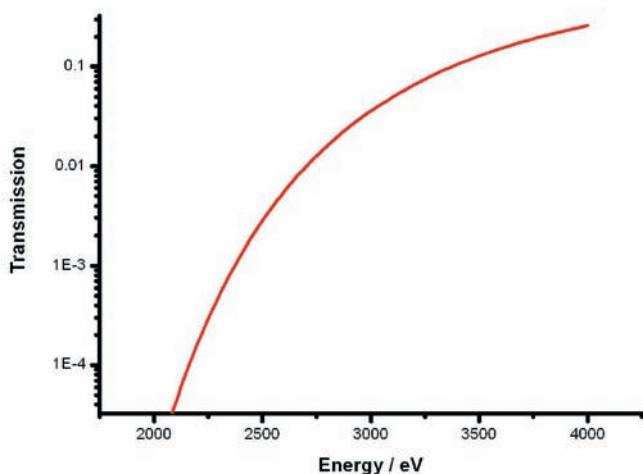


Figure 1: This curve demonstrates the extreme penalty suffered from the use of Be at lower energies – data for 850 μm thick window.

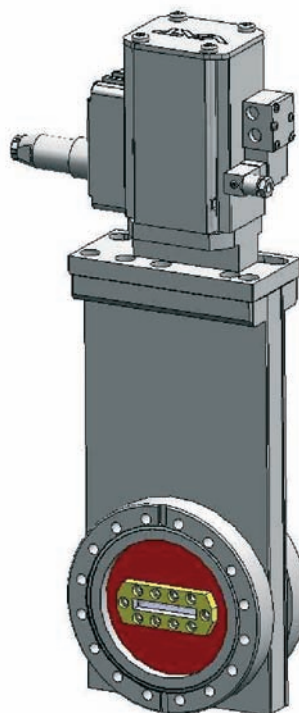


Figure 2: An illustration of a Be window installed in a gate valve.

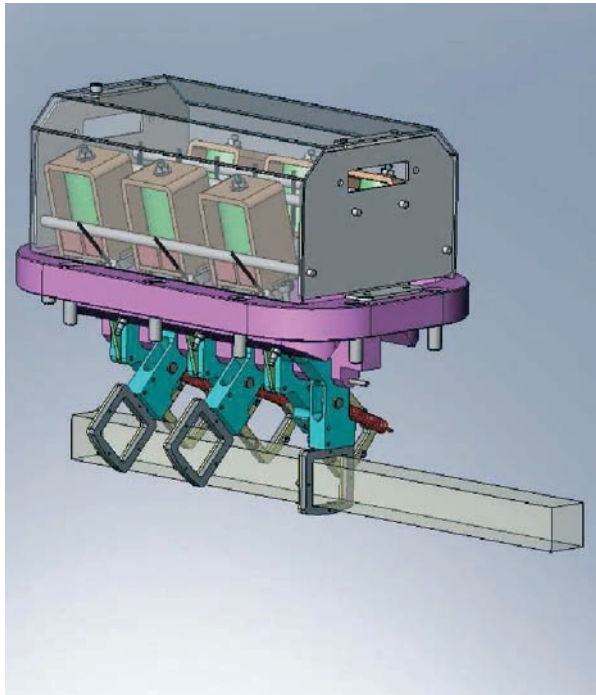


Figure 3

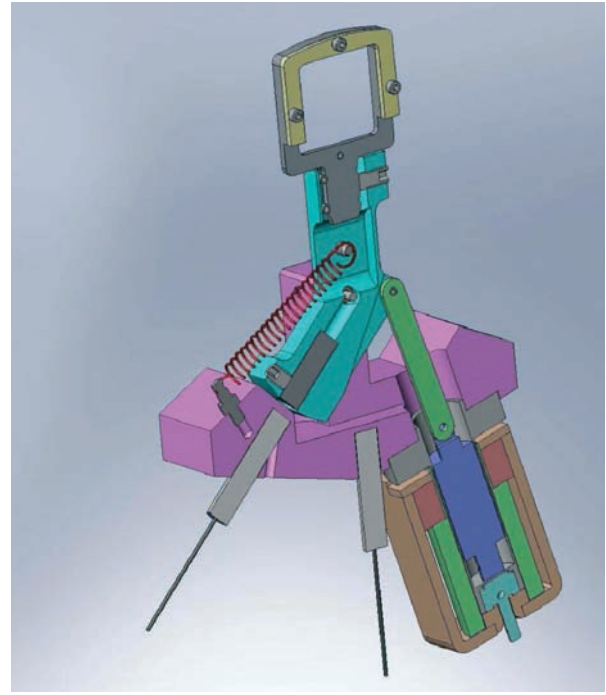
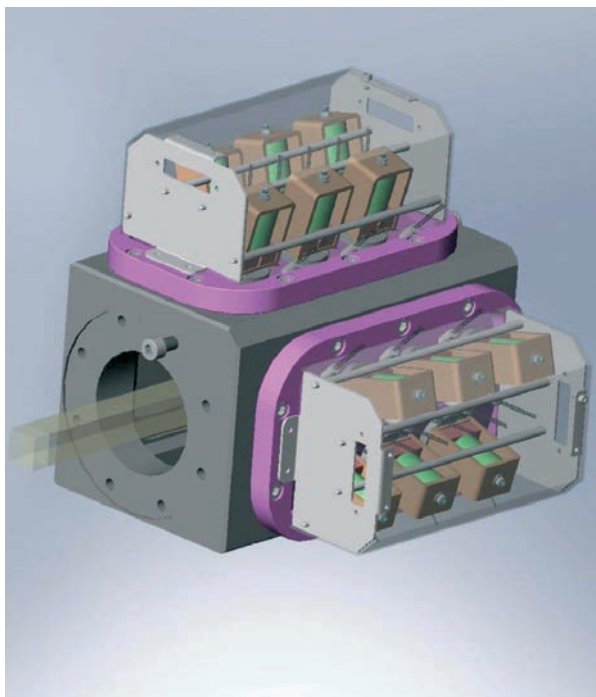


Figure 4

Figure 5



Figures 3-5: Illustrations of the new attenuators.



Figure 6: The vacuum-flange-mounted APD detector.

Temperature-induced changes in the atomic structure at the charged solid-liquid interface

Christopher Lucas, Paul Thompson, Ben Fowler, Michael Cormack, Alex Brownrigg, Vojislav Stamenkovi and Nenad Markovi—for further information contact CA Lucas, Oliver Lodge Laboratory, Department of Physics, University of Liverpool, Liverpool, L69 7ZE, UK.

clucas@liv.ac.uk

The electrochemical interface is important in a variety of scientific applications, for example, clean energy production and storage and photochemical energy conversion. At electrified solid-liquid interfaces, phenomena, such as surface restructuring and the adsorption of reactive and spectator species, give rise to a rich diversity of tunable ordered structures which determine both the reactivity and stability. While temperature effects on the kinetics of electrochemical reactions have routinely been examined in the past there has been no corresponding *in-situ* information on the temperature-induced changes in the atomic structures of either surface atoms or adsorbate layers. As a consequence, structure-function relationships have only been determined at room temperature. Although these studies have given valuable information, room temperature is far below the temperature range that is important for the development of more efficient and reliable energy conversion/storage technologies. Therefore we have developed a SXS electrochemical cell that incorporates temperature control over the range 273–360 K and this is shown schematically in Figure 1. Temperature control is achieved by a Peltier device attached to the base of the cell with the temperature being monitored by a thermocouple embedded in the cell wall. Preliminary measurements have focused on two canonical systems; the surface reconstruction of Au and the molecular adsorbate structures formed by CO on Pt. Figure 1 shows a schematic of the potential-dependent CO structures that are formed on

the Pt(111) electrode surface. Figures 2b and 2c show the x-ray voltammetry (XRV) data for the p(2x2) and $\sqrt{19}$ structures respectively at the three different temperatures. Fits to the rocking curves through the (1/2, 1/2) and (3/19, 14/19) CO reflections (measured at $l=0.2$) were obtained after potential cycling over the range 0.051.2 V and then holding at the fixed potential for ~5 minutes. Figures 2b, 2c show the integrated intensities and domain sizes (inversely proportional to the widths of the diffraction peaks) as a function of temperature for both CO structures. From these data it is apparent that the ordering of the p(2x2)-3CO structure is frustrated under both “cold” (280 K) as well as “hot” (319 K) conditions. The fact that the integrated intensities and the widths of the p(2x2) peaks show a “volcano” relationship with the temperature of electrolyte may indicate that the balance between the rate of CO ordering and the surface coverage by oxygenated species (rate of CO oxidation) reaches a maximum at room temperature (293 K). Note also that the potential window of stability of the p(2x2) structure (Figure 2b) decreases significantly by increasing the temperature, reflecting the negative shift in the onset of OH adsorption. In contrast to the p(2x2) structure, the ordering of the $\sqrt{19}$ structure (i.e. coherent domain size) increases linearly by increasing the temperature (from 4.7 nm at 279 K to 40 nm at 319 K). This may be due to the enhanced mobility of CO as the temperature increases which allows for the formation of larger domains of a structure which has a large unit cell. Most importantly, it can be seen that at 319 K (Figure 2c) the $\sqrt{19}$ phase exists even at the onset of the hydrogen evolution reaction (at ~0.05 V) and is coexistent with the p(2x2) phase.

The results show that a temperature change of *only* 40 K can alter the potential range of stability of adsorbate structures by over 1 V, i.e. a potential range encompassing *all* of the key potential-driven reactions on the Pt electrode surface. This demonstrates that temperature is an important parameter in the elucidation of structure-function relationships at electrified metal-liquid interfaces.

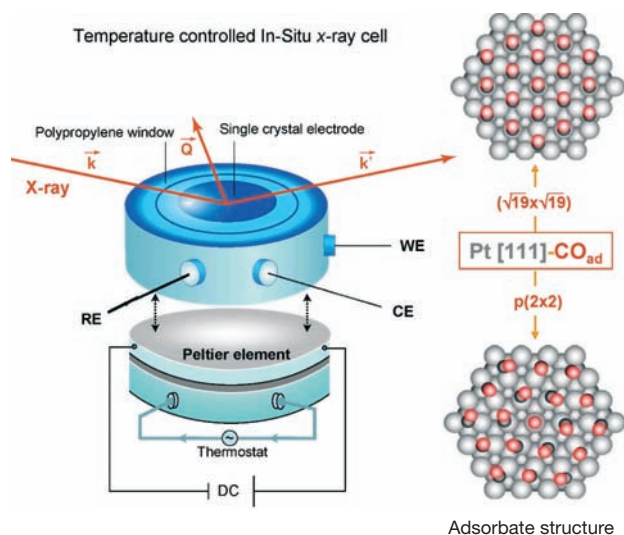


Figure 1: Schematic illustration of the experimental arrangement and the CO adlayers formed on the Pt(111) electrode. Temperature control in the x-ray scattering electrochemical cell is achieved by a Peltier element attached to the base. The CO adlayer structures can be directly measured by SXS as a function of both the applied electrode potential and temperature.



the examination of the temperature-dependent restructuring of metal surface atoms, oxide formation and adlayer structures of adsorbed spectator anions and cations would be of particular interest in the future. Such studies could provide a new dimension in the quest to develop a unified understanding of chemical bond making and bond making at temperatures that are relevant to the development of efficient energy conversion and storage systems.

Interplay of RE and Mn magnetism in multiferroic REMnO_3

E. Dudzik, R. Feyerherm, O. Prokhnenko, N. Aliouane, D. Argyriou, M. Mostovoy, L. Bouchenoire, S. Brown – for more information contact R. Feyerherm at Hahn-Meitner-Institute (HMI), Berlin, Germany.

feyerherm@hmi.de

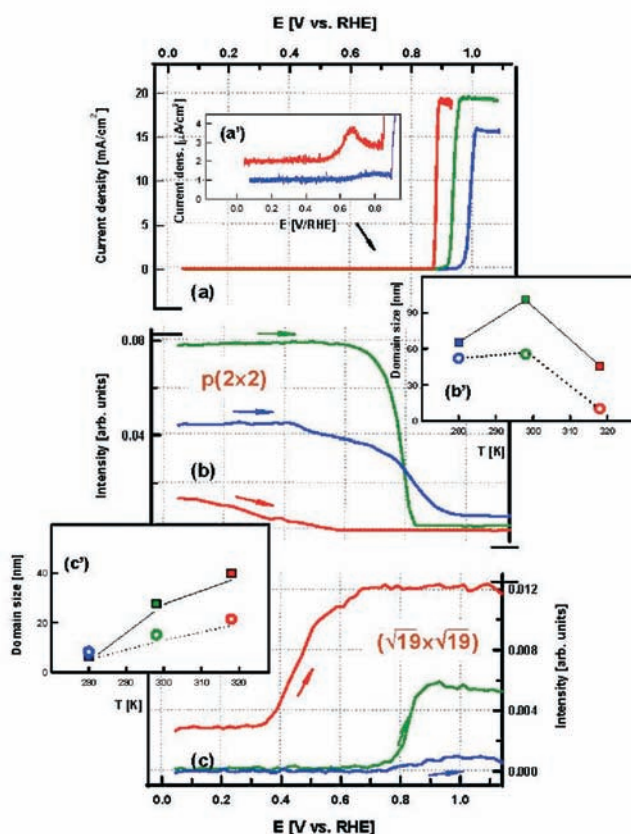


Figure 2: Temperature effects on the structure and oxidation of carbon monoxide on the Pt(111) electrode in 0.1 M HClO_4 . (a) Polarization curves indicating the temperature-controlled CO oxidation reaction in the pre-ignition potential region and at the ignition potential. At 279 K (blue data) the diffusion limiting current for CO oxidation is not reached. (a) Enlargement of the pre-ignition region showing enhanced CO oxidation at higher temperatures. (b) XRV measured at a CO- $p(2 \times 2)$ peak (only anodic sweeps are shown) as a function of temperature. (b) the integrated intensity (arb. units) and domain size (nm) of the CO- $p(2 \times 2)$ structure measured at 0.05 V as a function of temperature. (c) XRV measured at a CO- $\sqrt{19}$ peak (only anodic sweeps are shown) as a function of temperature. (c) the integrated intensity (arb. units) and domain size (nm) of the CO- $\sqrt{19}$ structure measured at 0.9 V as a function of temperature. At 319 K the $p(2 \times 2)$ and $\sqrt{19}$ structures are coexistent at 0.05 V whereas at 279 K the structures are coexistent at 0.9 V. Red data corresponds to data measured at 319 K, green data at 293 K (room temperature) and blue data at 279 K. The sweep rate in the electrochemical and SXS measurements was 2mV/s.

In multiferroics magnetism and ferroelectricity are closely entwined: magnetisation can be switched by an electric field, and an applied magnetic field may switch their electric polarisation. The orthorhombic rare earth manganites REMnO_3 with RE = Gd, Dy, and Tb belong to this group and show a complex interplay of magnetism and electric polarisation.

At room temperature these materials are paramagnetic and paraelectric. The first magnetic phase transition occurs around 40 K, where the Mn moments order in a sinusoidal spin density wave whose period changes with temperature. At a second transition the Mn order locks into a helicoidal spin density wave for RE = Dy and Tb, or into a simple commensurate state for RE = Gd. The RE ions order magnetically at temperatures below 10 K.

Both DyMnO_3 and TbMnO_3 show a spontaneous electric polarization below the intermediate lock-in transition. In previous zero-field X-ray resonant magnetic scattering (XRMS) studies, carried out at the HMI operated beamline MAGS at the Berlin synchrotron BESSY, we have demonstrated that in DyMnO_3 the magnetic polarization of the Dy ions induced by the Mn ordering leads to an effective enhancement of the electric polarisation. For TbMnO_3 , in turn, we have found a novel matching $3q_{\text{Tb}} - q_{\text{Mn}} = 1$ of the Tb and Mn ground state magnetic wave vectors, demonstrating a strong interplay of the two different types of magnetic ions.

Since the new 5T magnet at MAGS has not yet been commissioned, we decided to use XMaS with its 4 T superconducting magnet for field-dependent XRMS measurements on TbMnO_3 and GdMnO_3 . Notably, ferroelectricity in GdMnO_3 only occurs for applied magnetic fields $>1\text{T}$.

TbMnO_3 was known to exhibit a two-step metamagnetic transition for magnetic fields applied along the a axis, where the Tb moments are aligned ferromagnetically after the second step. For the intermediate field-range ($0.9\text{ T} < H_a < 1.4\text{ T}$) we found that Bragg reflections corresponding to the basic Tb ordering with wave vector $q_{\text{Tb}} = 3/7 b^*$ vanish while new reflections at $q_{\text{Tb}} = 0.361(1) b^*$ appear and q_{Mn} shifts from 0.285(1) to 0.276(1). This behaviour suggests that in applied magnetic field the two wave vectors become related by $2q_{\text{Tb}} + q_{\text{Mn}} = 1$.

Phenomenologically, the zero field behaviour results from the quartic coupling $gL^3_{\text{Tb}}L_{\text{Mn}}$ between the Tb and Mn magnetic order parameters, which favours a

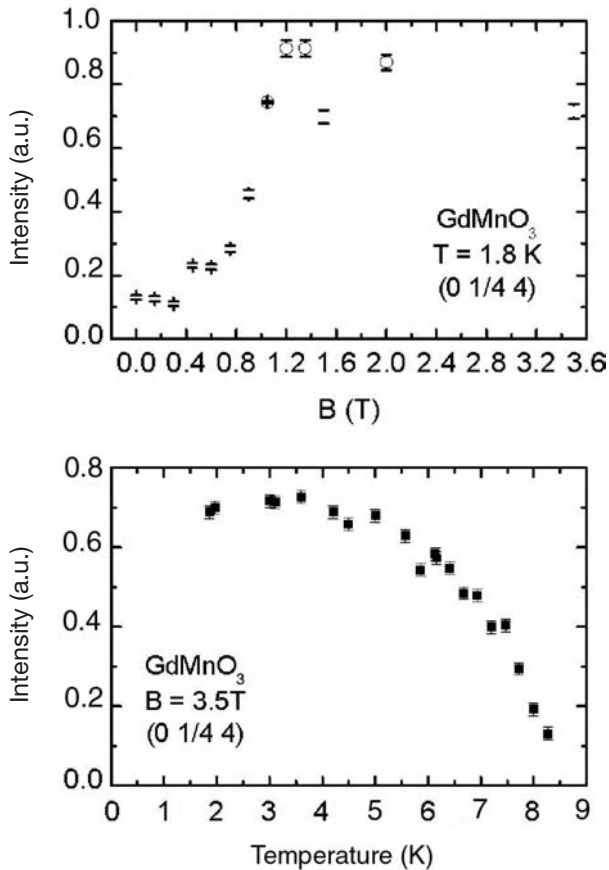


Figure 1: Magnetic field dependence of (top) the intensity of the Bragg reflection (0 1/4 4) at 1.8 K and (bottom) the temperature dependence at a field of 3.5 T, both measured at the Gd- L_{-3} edge in GdMnO₃.

relation $3q_{\text{Tb}} \pm q_{\text{Mn}} = n$ ($n = \text{integer}$) between the wave vectors of the two spin-density waves and, in particular, gives the observed relation $3q_{\text{Tb}} - q_{\text{Mn}} = 1$ for TbMnO₃ at $H = 0$. In an applied magnetic field H , the Tb spindensity wave acquires a homogeneous component cH and the quartic term effectively leads to the coupling $3gcHL^2_{\text{Tb}}L_{\text{Mn}}$ favouring $2q_{\text{Tb}} \pm q_{\text{Mn}} = n$, explaining the switch of the relation between the Tb- and Mn-ordering wave vectors observed for $H \parallel a$ (see PRL 99, 177206 (2007)).

For GdMnO₃ we also observe a unique behaviour. While the Mn moments are ordered in a simple antiferromagnetic “A-type” pattern ($q_{\text{Mn}} = 0$) in zero magnetic field below the lockin temperature of 23 K, we find that the Gd moments order separately with a propagation vector $q_{\text{Gd}} = 1/4 b^*$ below 6 K. Notably, this is the same propagation vector that was reported for the Mn moments in an applied magnetic field $\parallel b$, $H_b > 1$ T, for temperatures below about 10 K. Again, this indicates an intricate relation between the two different types of magnetic ions in GdMnO₃.

Figure 1 shows the magnetic field dependence of the intensity of the Bragg reflection (0 1/4 4) at 1.8 K and the temperature dependence at a field of 3.5 T, both measured at the Gd L_{-3} edge. The scattering

geometry was chosen so that the magnetic field was tilted only a few degrees from the b axis.

We associate the finite zerofield intensity of the reflection (0 1/4 4) with the $q_{\text{Gd}} = 1/4 b^*$ magnetic ordering of Gd moments. For $H_b > 1$ T, the Mn moments order with the same propagation vector and apparently induce a significant polarisation of the Gd 5d electrons, leading to a strong enhancement of the observed Bragg intensity. In this state, GdMnO₃ is ferroelectric. The temperature dependence for $H = 3.5$ T shows that the $q_{\text{Mn}} = 1/4 b^*$ ordering breaks down at about 8.5 K, i.e., at the transition to the paraelectric state.

In this context it is intriguing that magnetisation measurements indicate that for $H_b > 1$ T the Gd 4f moments are ferromagnetically aligned. This would imply that the Mn moments take over the $1/4 b^*$ ordering from the Gd once the corresponding Gd ordering is destroyed by the applied magnetic field. Further studies may help clarifying.

Profiling the induced 5f polarisation in U/Fe multilayers, using XRMR

R. Springell, S. D. Brown, L. Bouchenoire, P. Thompson, A. Mirone, W. G. Stirling, A. Beesley, M. F. Thomas, R. C. C. Ward, M. R. Wells, S. Langridge, S. W. Zochowski and G. H. Lander – for further information contact R. Springell at the ESRF, Grenoble, 38000, France.

ross.springell@esrf.fr

Magnetic multilayers have now become commonplace for investigating electronic interactions at metallic interfaces. Indeed, some unique combinations of materials have led to novel coupling phenomena that have important technological applications today. The understanding of such mechanisms has been the subject of the recent Nobel Prize in Physics. Our interest lies in the fundamental nature of interactions between the U 5f and Fe 3d electronic states in U/Fe multilayers, particularly concerning the magnetism of uranium.

The samples were prepared at the Clarendon Laboratory, University of Oxford, using dc magnetron sputtering in a loadlocked UHV chamber. The multilayers were grown on (11.0) sapphire substrates with niobium buffer and capping layers. Bulk magnetisation and laboratory-based X-ray scattering techniques carried out on these multilayers indicated that the interfaces consisted of diffused regions or mixtures of uranium and iron.

We have employed the X-ray resonant magnetic reflectivity (XRMR) technique at the XMaS beamline to describe more fully the multilayer structure, to detect induced U 5f polarisation and to determine its spatial dependence. By measuring the reflectivity



across the U M_4 edge (3728 eV), which probes transitions from $3d_{3/2}$ core levels to empty $5f_{5/2}$ states, resonant enhancements in the scattering factor dramatically improve the chemical contrast and magnetic dichroism can be detected with the employment of circularly polarised X-rays (XMCD).

The X-ray reflectivity data was collected, while reversing the magnetic field, to measure simultaneously the charge and magnetic-charge interference scattering. Figure 1 shows the experimental data and fitted calculations at four example energies (of a total of 17) for sample SN71, nominally $[U_9/Fe_{34}]_{30}$. The sampling of such a large number of energies allowed us to precisely model the imaginary part of the charge and magnetic scattering factors, directly related to the fluorescence and the XMCD absorption coefficient, respectively. The calculations used to reproduce the experimental data included a number of parameters used to describe the interfacial structure and the variation in the U polarisation within the bilayer, see Figure 2.

The observation of an induced magnetisation within the U layers in U/Fe multilayers and the shape of the profile, the majority of the polarisation closest to the bcc iron and in the same direction at each interface, is in close agreement with theoretical predictions.

Future measurements are now planned to investigate the U/Gd multilayer system.

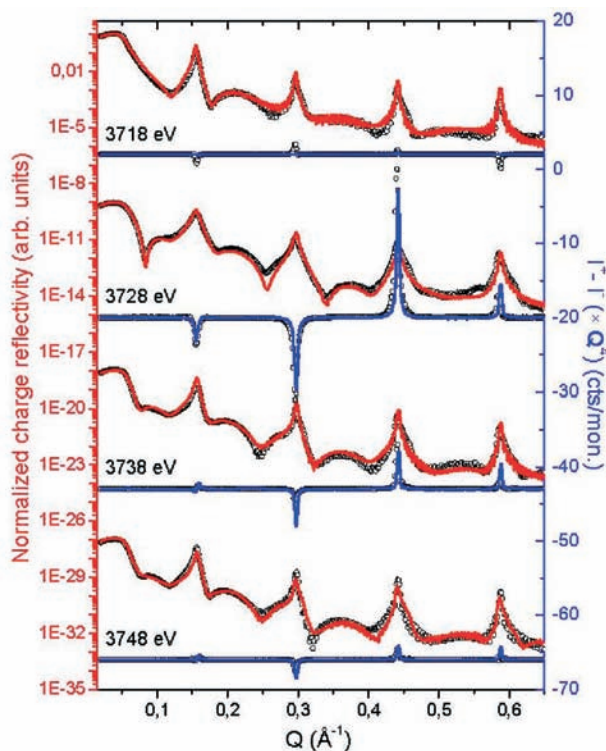


Figure 1: The charge reflectivity and the magnetic-charge interference scattering (scaled by a Q^4 factor) are shown for four energies across the U M_4 edge. The data are shown as the open black circles and the fitted calculations are represented by the solid red and blue lines.

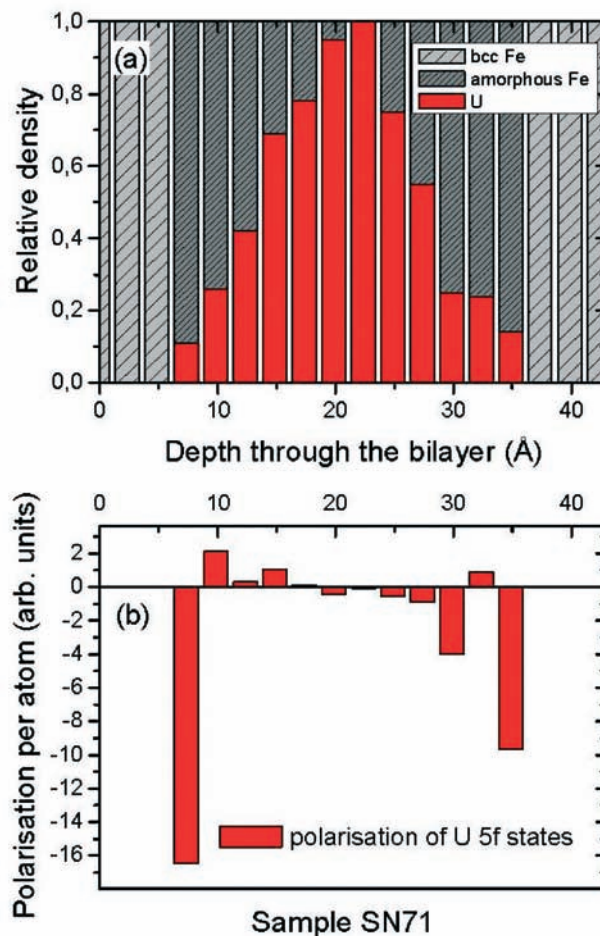


Figure 2: Profiles of the relative uranium and iron densities as a function of bilayer depth are shown in panel (a). Panel (b) presents the profile of the U 5f polarisation.

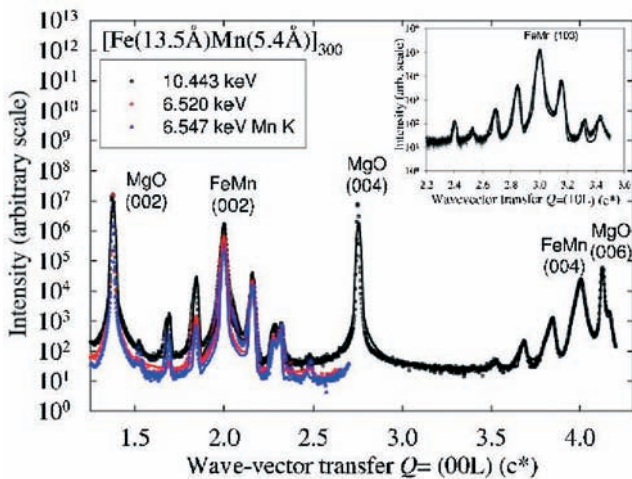
Perpendicular antiferromagnetic ordering of Mn and exchange anisotropy in Fe/Mn multilayers

S. J. Lee, J. P. Goff, G. J. McIntyre, R. C. C. Ward, S. Langridge, T. Charlton, R. Dalglish, D. Mannix – for further information contact J. P. Goff at Department of Physics, Royal Holloway, University of London, Egham TW20 OEX, UK.

jon.goff@rhul.ac.uk

There has been intense interest in the exchange-bias phenomenon in recent years due to its importance in technological applications, such as read heads, sensors, and magnetic random access memory. Bias fields arise from the interaction between ferromagnetic (FM) and antiferromagnetic (AF) components, but these fields are an order of magnitude smaller than expected using simple microscopic models. Fe/Mn multilayers are model systems in which to study exchange bias, since the AF Mn layers have uncompensated moments. We have determined the interfacial structures using the XMaS UK-CRG at the ESRF, and the magnetic ordering at the ILL and ISIS. The one-electron

contrast between the two constituents of the multilayers means that the anomalous dispersion can be used to vary the scattering contrast as a function of x-ray energy at the Fe and Mn K edges, allowing severe constraint of the structural model. The completely unexpected orthogonal magnetic structures can be explained by the frustration of the interfacial interaction due to the terracing determined using x-rays. The results readily explain why the bias fields are so small, and show that the microscopic magnetic ordering assumed in a variety of exchange-biased systems may have to be revised.



The role of pre-oxidation on the interface structure of Co/MgO multilayers

D. S. Eastwood, W. F. Egelhoff Jr., B. K. Tanner – for further information contact: D. S. Eastwood at Department of Physics, University of Durham, DH1 3LE, UK

d.s.eastwood@durham.ac.uk

Pre-oxidation of the bottom electrode of a magnetic tunnel junction (MTJ) in a low pressure of oxygen prior to depositing the oxide barrier layer has been shown to result in a major reduction in the coupling field between electrodes for both alumina and MgO based MTJ structures.

We used the Mar CCD camera to measure the diffuse scatter and hence to determine interface parameters of MTJs and Co/MgO multilayers. By fitting the amplitude of Bragg peaks caused by the repeated interfaces (as labelled in Fig. 1), we observed very different in-plane correlation cut-off lengths for the different sample preparation methods. From the linear fits to these data in Fig. 2, we were able to deduce that the in-plane length is reduced from 4 nm to 2 nm with use of the pre-oxidation technique. This finding will improve our understanding of the magnetic behaviour, and allow further enhancement of the low-field sensitivity of these devices.

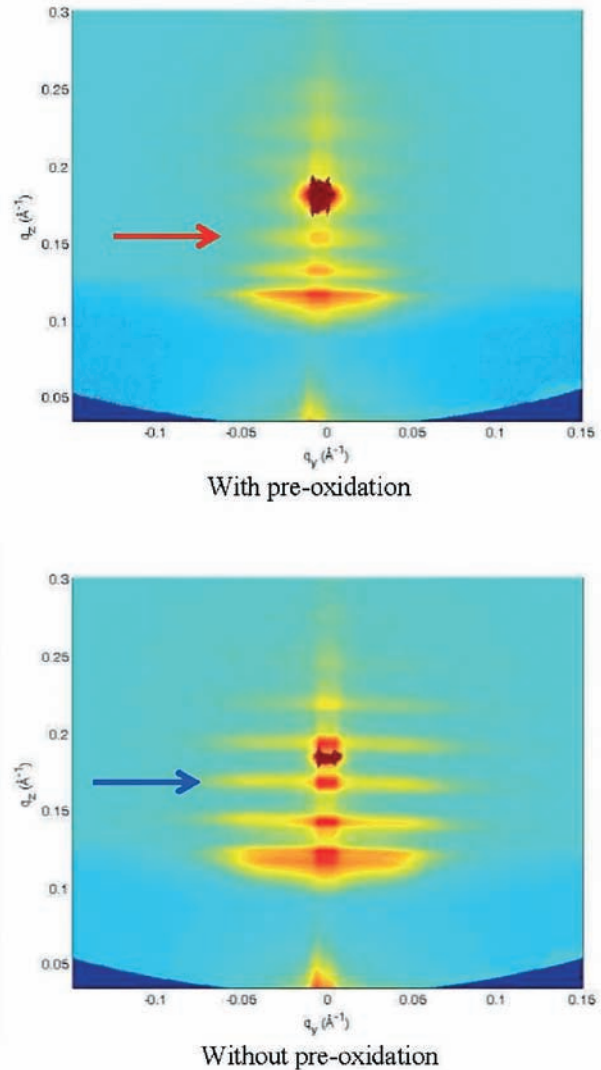


Figure 1: CCD images of diffuse scatter from Co / MgO multilayer structures. The extent of the labelled Bragg peaks in the q_y direction indicates a very different scaling behaviour for the interface structures of the pre-oxidised and un-pre-oxidised interfaces.

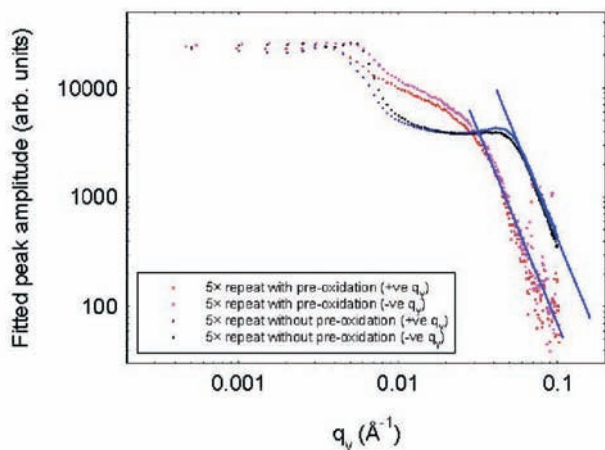


Figure 2: The fitted amplitude of the 1st Bragg peak in Fig. 1, as a function of the lateral in-plane coordinate q_y .



Combined x-ray interaction data for biological tissue classification in secondary colorectal liver cancer

Michael Farquharson, City Community and Health Sciences, City University, London

m.j.farquharson@city.ac.uk

This was a feasibility study on liver tissue classification using our proposed x-ray interaction techniques. The experiment consisted of obtaining diffraction, Compton scatter and XRF data. The samples were 30 matched pairs of liver, each pair consisting of a sample of secondary colorectal liver cancer and a piece of tissue taken at a distance from the cancer in the same liver, the latter being classified as normal. Once back in the UK histopathology analysis was undertaken.

Diffraction data. Figure 1 shows the average diffraction data for the normal samples and tumour samples. It can clearly be seen that between scatter angles 5 degrees to approximately 20 degrees there is a difference in the intensity of the signal. The increase seems to be centred around a scatter angle of 12-13 degrees. This is the value for the response from adipose (fat) tissue, which would indicate that tumour tissue has a decreased level of fat tissue compared to that of the normal tissue in the same liver.

XRF (Elemental analysis) data. Figure 2 shows the average X-ray fluorescence spectra for the normal and the tumour samples. From previous work on breast tissue and the advice of our clinical collaborators, the elements of interest in this study are potassium (3.2 keV); iron (6.4 and 6.9 keV), copper (8 keV) and zinc (8.6 and 9.5 keV).

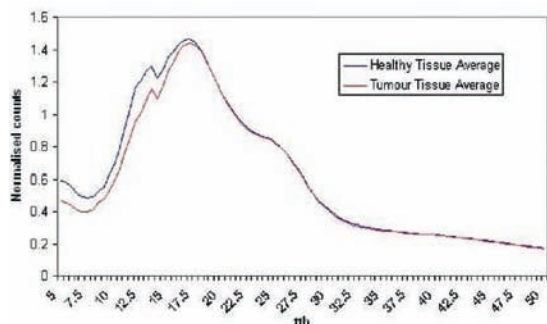


Figure 1: Averaged normal and averaged tumour response.

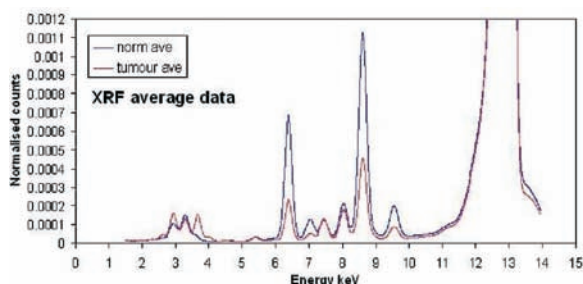


Figure 2: Averaged spectra for normal and tumour samples.

Compton Scatter (electron density) data. Figure 3 shows the average response for the Compton scatter measurements. It can be seen that there appears to be no difference in this measurement at all between the normal and tumour samples.

The diffraction data and the xrf data were combined in two simple ways in order to see how they performed as a tissue predictor. (A subset of 5 normals and 5 tumours were used at test objects.) The model in figure 4 used fitted peak data from the XRF measurements and a simple summation of a region of the diffraction data as well as the physical density of the sample as an additional variable. In this particular representation all samples should ideally have a value of 1.

This summarises the **preliminary** analysis of the data obtained at BM28 on liver samples. It can be clearly seen that the measurement parameters appear to offer tissue classification abilities. The data needs much closer inspection before the full potential of these results is seen. One important consideration is the presence of certain outliers within the sample population. The PCA analysis did pick these out and they have been removed in the above figures. However histopathology reports have shown that 1 sample matched pair was labelled the wrong way round and a further 3 samples were necrotic tissue which could not be used. We are now working closely with our clinical partners, the Royal Free NHS Trust, London and the results we have obtained to date and the experienced gained for our work on BM28 have enabled us to design a laboratory set up that could be used to discriminate tumour from normal tissue which would have great benefit in the determination of margin identification in cancer surgery.

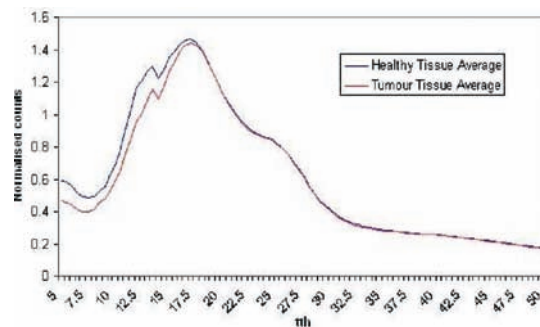


Figure 3: Averaged Compton scatter response for the normal and tumour samples.

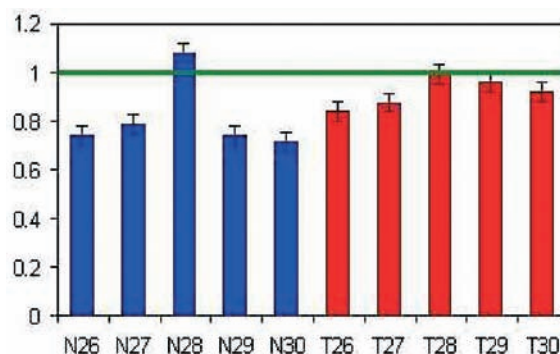


Figure 4: Predictions for 5 normal and 5 tumour samples. All samples should ideally have a value of 1.

eCell on XMaS: time resolved spectroelectrochemistry and corrosion of real metal surfaces

M. G. Dowsett, A. Adriaens, G. K. C. Jones and L. Bouchenoire – for further information contact M. G. Dowsett, Department of Physics, University of Warwick, Coventry, CV4 7AL UK

m.g.dowsett@warwick.ac.uk

We have successfully deployed a new environmental cell (eCell) on XMaS, capable of maintaining a controlled liquid, gas or vapour environment over a sample. (Fig. 1) The eCell is a second generation of a published design and is especially configured to take advantage of the Mar CCD 165 camera in surface diffraction experiments. It can function as a three electrode electrochemical cell when filled with liquid electrolyte, allowing time-resolved spectro-electrochemistry (Fig. 2) with an XRD time resolution of ~12 sec (limited by the readout speed of the Mar). To ensure that x-rays can

reach the sample surface, and that electrochemical and solution processes can take place undistorted by limited electrolyte volumes, the working electrode can be raised and lowered between “x-ray” and “electrochemistry” positions under remote control. In the former position, about 125 mm of electrolyte remains between the sample surface and an 8 mm thick Kapton x-ray window. In the latter, the electrolyte thickness increases to ~5 mm. Mar image acquisition can now be triggered from out control system when the sample is in the x-ray position. The eCell has also been used to expose protected and unprotected metal surfaces to a corrosive gas, and the movement of the sample has been exploited to examine the action of a corrosive liquid on a metal in its earliest stages as follows: A droplet of the corrosive fluid is placed on the inside surface of the x-ray window, where it remains suspended. The sample is initially in the “electrochemistry” position, clear of the droplet. It is then rapidly raised to the “x-ray” position, squashing the droplet against the window and rapidly wetting the metal surface; an image sequence is initiated at the same time.

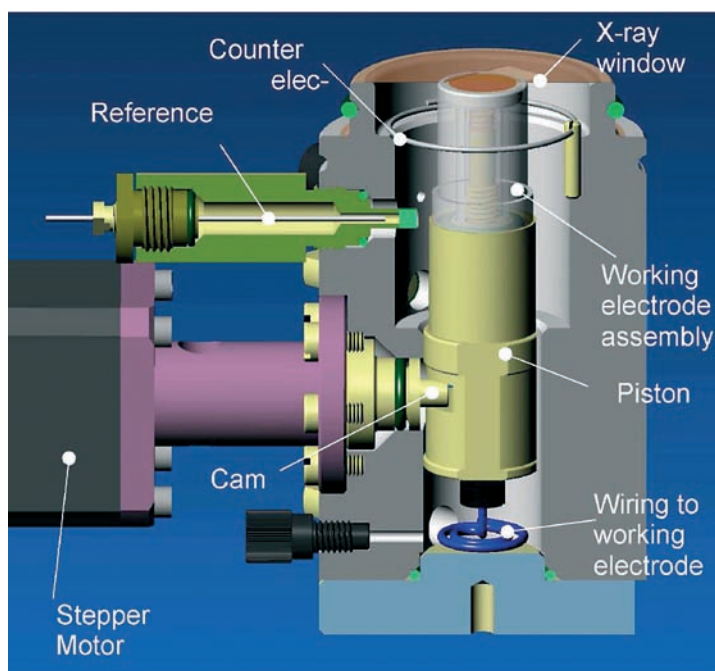


Figure 1: Cut-away view of eCell; designs ©2005 Eva Surface Analysis.

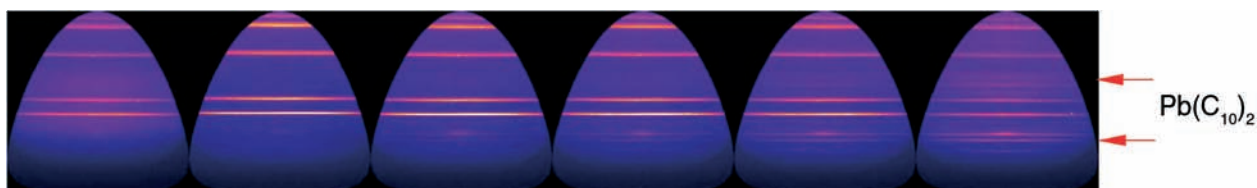


Figure 2: Reprojected Mar CCD image sequence (movie) showing growth of a lead decanoate film on a lead surface ($\text{CH}_3(\text{CH}_2)_8\text{COO})_2\text{Pb}=\text{Pb}(\text{C}_{10})_2$) for the protection of heritage lead.



Detailed analysis of the spectral line shape of holmium at the L_3 edge

L. Bouchenoire, A. Mirone, S.D. Brown, P. Strange, T. Wood, P. Thompson and D. Fort for further information contact L.Bouchenoire at XMaS, ESRF, F38043 Grenoble

boucheno@esrf.fr

The angular and polarization dependence of the electric dipolar (E1) and quadrupolar (E2) contributions to the scattering cross-section was studied for the first time taking into account a double dipole feature in basal plane spiral antiferromagnetic holmium at the L_3 edge. The experimental line shapes were corrected for the Lorentz factor, the beam divergence and the sample absorption. The latter is the most crucial correction as its under/over estimation could lead to a completely wrong determination of the relative amplitudes between the E1 ($F_{E1}^{(1)}$) and E2 ($F_{E2}^{(1)}$ and $F_{E2}^{(3)}$) scattering factors. These factors have been extracted individually by fitting Lorentzian functions to the experimental line shapes as a function of energy (Figure 2).

The fits unambiguously confirmed that the low energy peak observed in the energy line shapes of the heavy rareearths originates from mixed E1 and E2 excitations (see article by S. Brown et al., Newsletter 2005). The main E1 peak corresponds to the energy of Feature A in Figure 1. The other peak resonates ~ 1 eV below the E2 contribution and is not negligible. This peak results from the hybridization between the $5d$ and $4f$ states. Band structure calculations have also predicted a split d -band, with the lower energy E1 peak around the same energy as the E2 contribution although this prediction was made for a

c-axis moment. The ratio $F_{E2}^{(3)}/F_{E2}^{(1)}$ was found to be ~ 0.38 and smaller than the free-ion value of 0.5.

The results demonstrate that a complete polarisation analysis of the RXMS is a valuable technique which allows us to accurately identify all the resonance processes and quantify each scattering term that takes place. ■

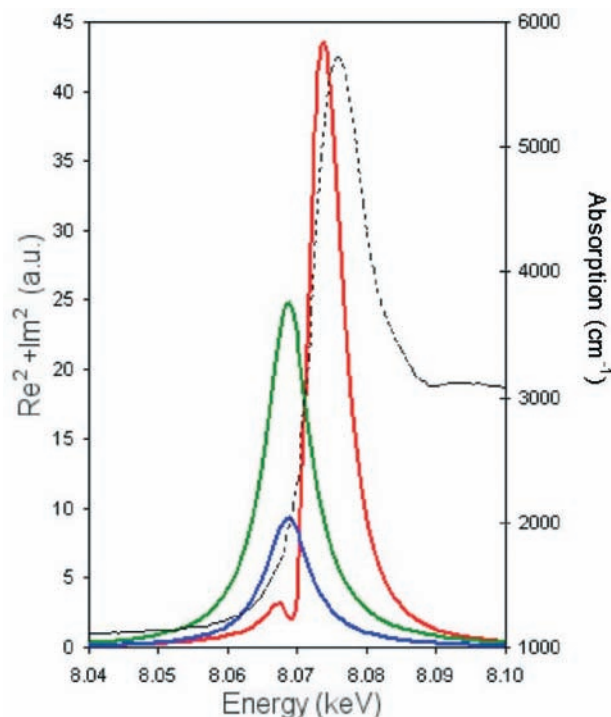


Figure 2: Modulus squared of the scattering factors: $F_{E1}^{(1)}$ (red), $F_{E2}^{(1)}$ (green) and $F_{E2}^{(3)}$ (blue). The black line is the absorption curve measured through a 5 mm thick Ho foil.

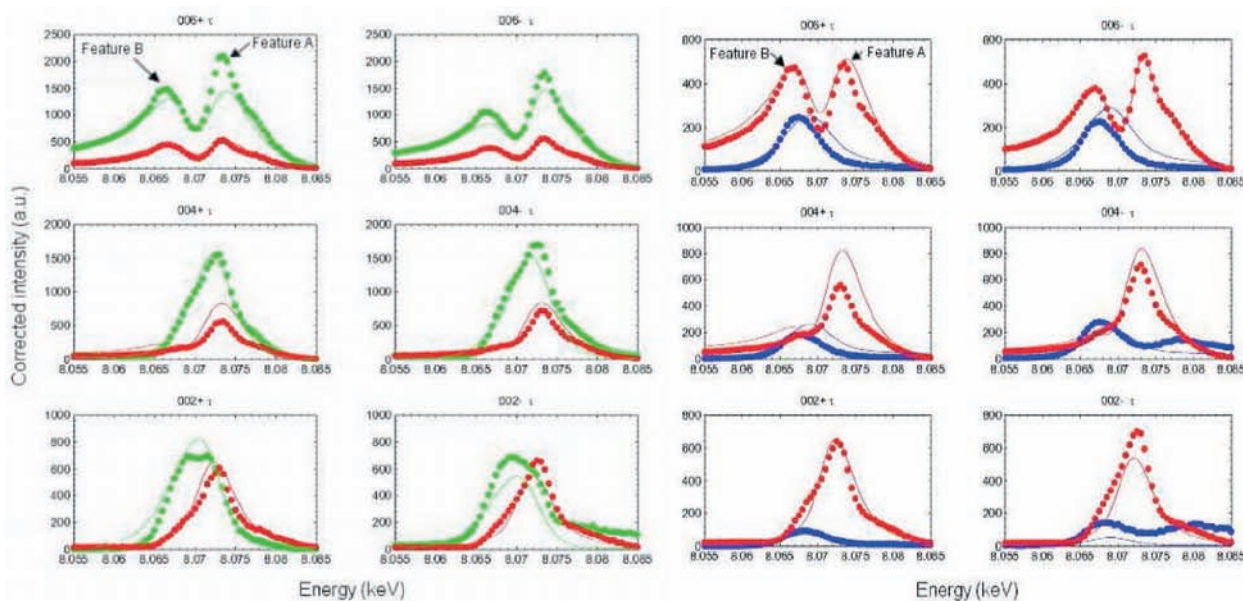


Figure 1: Measured resonant line shapes (circles) across the Ho L_3 edge in $\pi \rightarrow \pi$ (green), $\pi \rightarrow \sigma$ (red) in $\sigma \rightarrow \sigma$ (blue), $\sigma \rightarrow \pi$ (red) and comparison to fits (lines).

➔ Please note

Some of the experimental reports in the previous pages are as yet unpublished. Please email the contact person if you are interested in any of them or wish to quote these results elsewhere.

➔ Our web site

This is at:

<http://www.esrf.fr/UsersAndScience/Experiments/CRG/BM28/>

It contains the definitive information about the beamline and an online beamline manual.

➔ Living allowances

These are still 55 euros per day per beamline user – the equivalent actually reimbursed in pounds sterling, of course. XMaS will support up to 3 users per experiment. This is not a restriction on the number of experimentalists but you should make your own budgetary arrangements for those in excess of 3. The ESRF hostel still appears adequate to accommodate all our users, though CRG users will always have a lower priority than the ESRF's own users. Do remember to complete the webbased "A form" requested of you when you receive the ESRF invitation, all attendees must be listed, since this informs the safety group of the attendees and is used to organise all site passes, meal cards and accommodation.

➔ Beamline people

There have been two changes in the beamline staff since the last Newsletter – see under Beamline Scientists below.

➔ Project Co-ordinator

David Paul, (dpaul@esrf.fr), is the person who can provide you with general information about the beamline, application procedures etc. David should normally be your first point of contact.

➔ Beamline Scientists

As mentioned on page 2 of this newsletter Danny Mannix, who has been part of the team since April 2001, left us in the autumn and his replacement, Peter Normile (normile@esrf.fr), took up his post at the beginning of February 2008. Simon Brown (sbrown@esrf.fr) and Laurence Bouchenoire (boucheno@esrf.fr) continue as beamline scientists.

➔ Technical Support

Paul Thompson (thompso@esrf.fr) continues to work on instrument development and provides technical support for the beamline. John Kervin (jkervin@liv.ac.uk), who is based at Liverpool University, provides further technical backup and spends part of his time onsite at XMaS.

➔ Project Directors

Malcolm Cooper (m.j.cooper@warwick.ac.uk) and Chris Lucas (clucas@liv.ac.uk) continue to travel between the UK and France to oversee the operation of the beamline. The administration for XMaS continues to be handled by Sandra Beaufoya t Warwick University (s.beaufoy@warwick.ac.uk).

➔ The Project Management Committee

The current membership of the committee is as follows: Bob Cernik (chair) Denis Greig Peter Hatton Colin Norris David Bradley Andrew Boothroyd Chris Nicklin Jonathan Williams (replacing Simon Crook) Meeting twice a year, in addition to the above, the directors, the chair of the PRP and the beamline team are in attendance.

➔ The Peer Review Panel

The current membership of the panel is as follows: Sean Langridge (chair) Paul Strange Carsten Detlefs Steve Collins Pam Thomas Ian Hamley Karen Edler In addition either Malcolm Cooper or Chris Lucas attend their meetings.

➔ Housekeeping!!

We take some trouble to keep the beamline clean and tidy, please leave the beamline in the same state! At the end of your experiment samples should be removed from cryostat and other sample environment mounts, tools, etc returned to racks and unwanted materials disposed of in an appropriate manner. When travel arrangements are made, therefore, please allow additional time, at the cessation of beam, to effect a tidyup.

➔ PUBLISH PLEASE!!... ...and keep us informed

Although our list of papers reporting work on XMaS is growing we still need more of those publications to appear. We ask you to provide Sandra Beaufoya not only with the reference but also a preprint/reprint for our growing collection. Note that the abstract of a publication can also serve as the experimental report!

➔ IMPORTANT!

When beamline staff have made a significant contribution to your scientific investigation you may naturally want to include them as authors. Otherwise we ask that you add an acknowledgement, of the form:

"This work was performed on the EPSRC-funded XMaS beam line at the ESRF, directed by M.J. Cooper and C.A. Lucas. We are grateful to the beam line team of S.D. Brown, D.F. Paul, P. Normile, L. Bouchenoire and P. Thompson for their invaluable assistance, and to S. Beaufoya and J. Kervin for additional support." ■



Guidelines for Applying for Beam-time at the XMaS beamline

Beamline Operation

The XMaS beamline at the ESRF, which came into operation in April 1998, has some 133 days of beam time available each year for UK user experiments, after deducting time allocated for ESRF users, machine dedicated runs and maintenance days. During the year, two long shut-downs of the ESRF are planned: 5 weeks in winter and 4 weeks in summer. At the ESRF beam is available for user experiments 24 hours a day.

Applications for Beam Time

Two proposal review rounds are held each year, with deadlines for submission of applications, normally, the end of **March** and **September** for the scheduling periods August to end of February, and March to July, respectively. **Applications for Beam Time** are to be submitted **electronically** (the paper versions are not acceptable) following the successful model used by the ESRF and ourselves. Please consult the instructions given in the ESRF web page:

www.esrf.fr

Follow the links: “**User Guide**”
And: “**Applying for Beam Time**”

Follow the instructions carefully – you must choose “XMAS-BM28” and “CRG Proposal” at the appropriate stage in the process. A detailed description of the process is always included in the reminder that is emailed to our users shortly before the deadline – for any problems contact D. Paul, as above.

Technical specifications of the Beamline and instrumentation available are described in the XMaS web page.

When preparing your application, please consider the following:

➔ All sections of the form must be filled in. Particular attention should be given to the safety aspects, and the name and characteristics of the substance completed carefully. Experimental conditions requiring special safety precautions such as the use of lasers, high pressure cells, dangerous substances, toxic substances and radioactive materials,

must be clearly stated in the proposal. Moreover, any ancillary equipment supplied by the user must conform with the appropriate French regulations. Further information may be obtained from the ESRF Experimental Safety Officer, tel: +33 (0)4 76 88 23 69; fax: +33 (0)4 76 88 24 18.

➔ Please indicate your date preferences, including any dates that you would be unable to attend if invited for an experiment. This will help us to produce a schedule that is satisfactory for all.

➔ An experimental report on previous measurements must be submitted. New applications will not be considered unless a report on previous work is submitted. These also should be submitted electronically, following the ESRF model. The procedure for the submission follows that for the submission of proposals – again, follow the instructions in the ESRF’s web pages carefully. Reports must be submitted within 6 months of the experiment.

➔ The XMaS beamline is available for one third of its operational time to the ESRF’s user community. Applications for beamtime within that quota should be made in the ESRF’s proposal round – **Note: their deadlines are earlier than for XMaS! – 1st March and 1st September.** Applications for the same experiment may be made both to XMaS directly and to the ESRF. Obviously proposals successfully awarded beamtime by the ESRF will not then be given beamtime additionally in the XMaS allocation.

Assessment of Applications

The Peer Review Panel for the UK-CRG considers the proposals, grades them according to scientific excellence, adjusts the requested beam time if required, and recommends proposals to be allocated beam time on the beamline.

Proposals which are allocated beam time must in addition meet ESRF safety and XMaS technical feasibility requirements.

Following each meeting of the Peer Review Panel, proposers will be informed of the decisions taken and some feedback provided. ■

XMaS Pluo B3, ESRF, BP 220, 38043 Grenoble Cedex, France
Tel: +33 (0)4 76 88 24 36 – Fax: +33 (0)4 76 88 24 55
Web page : http://www.esrf.fr/exp_facilities/BM28/xmas.html
Email: dpaul@esrf.fr



is an EPSRC sponsored project

